Mon. Not. R. Astron. Soc. **318**, 341–353 (2000)

Time-series spectroscopy of the rapidly oscillating Ap star HR 3831

Ivan K. Baldry[1,2]★ and Timothy R. Bedding[1]
[1]*Chatterton Astronomy Department, School of Physics, University of Sydney, NSW 2006, Australia*
[2]*Anglo-Australian Observatory, P.O. Box 296, Epping, NSW 1710, Australia*

Accepted 2000 April 14. Received 2000 April 10; in original form 2000 January 24

ABSTRACT

We present time-series spectroscopy of the rapidly oscillating Ap (roAp) star HR 3831. This star has a dominant pulsation period of 11.7 min and a rotation period of 2.85 d. We have analysed 1400 intermediate-resolution spectra of the wavelength region 6100–7100 Å obtained over one week, using techniques similar to those we applied to another roAp star, α Cir.

We confirm that the Hα velocity amplitude of HR 3831 is modulated with rotation phase. Such a modulation was predicted by the oblique pulsator model, and rules out the spotted pulsator model. However, further analysis of Hα and other lines reveals rotational modulations that cannot easily be explained using the oblique pulsator model. In particular, the phase of the pulsation as measured by the width of the Hα line varies with height in the line.

The variation of the Hα bisector shows a very similar pattern to that observed in α Cir, which we have previously attributed to a radial node in the stellar atmosphere. However, the striking similarities between the two stars, despite the much shorter period of α Cir (6.8 min), argues against this interpretation unless the structure of the atmosphere is somewhat different between the two stars. Alternatively, the bisector variation is a signature of the degree ℓ of the mode and not the overtone value n.

High-resolution studies of the metal lines in roAp stars are needed to understand fully the form of the pulsation in the atmosphere.

Key words: techniques: spectroscopic – stars: chemically peculiar – stars: individual: HR 3831 – stars: oscillations – stars: variables: other.

1 INTRODUCTION

The rapidly oscillating Ap (roAp) stars pulsate in high-overtone non-radial p-modes (Kurtz 1990; Martinez & Kurtz 1995; Matthews 1991, 1997; Shibahashi 1991). The oscillation spectra of many of these stars reveal frequency multiplets – usually triplets – with equal frequency separations of the components. The separations are equal to, or very nearly equal to, the rotation frequency (determined from the variation of spectrum and light as the star rotates).

One explanation of the observed triplets is that a set of rotationally perturbed m-modes is excited, e.g., $\ell = 1$ dipole modes with $m = -1,\ 0,\ +1$. The observed frequencies can be written as

$$\nu_m = \nu_0 - m(1 - C_{n\ell})\nu_{\rm rot} \qquad (1)$$

where $C_{n\ell}$ is a constant that depends on the structure of the star (Ledoux 1951). For A-star models with the expected pulsation modes for roAp stars, Takata & Shibahashi (1995) found $C_{n\ell} \approx 0.003$–0.010. However, in the best-observed roAp star HR 3831, Kurtz et al. (1992) were able to show that $C_{n\ell} < 2 \times 10^{-5}$. This is two orders of magnitude less than the lowest theoretically predicted values, and suggests that the frequency splitting is precisely the rotational frequency.

Another explanation for a frequency multiplet is a single pulsation mode (e.g., $\ell = 1$, $m = 0$) the amplitude of which is modulated[1] by rotation. This naturally produces a frequency splitting that is precisely equal to the rotation frequency. In some roAp stars, the amplitude of the pulsation has been observed to modulate with rotation *in phase* with the magnetic variation. To explain this phenomenon, the oblique pulsator model was proposed by Kurtz (1982), and has been extensively developed by Shibahashi & Takata (1993; Takata & Shibahashi 1994, 1995). In this model, the magnetic and pulsation axes are aligned but are oblique to the rotation axis. The observed amplitude modulation is then a result of the variation in the angle between the pulsation axis and the line of sight as the star rotates.

★ E-mail: baldry@aaoepp.aao.gov.au (IKB)

[1] In this paper, we use *modulation* to describe changes in amplitude and phase with rotation, and *variation* for other types of changes.

In an alternative model, the spotted pulsator model (Mathys 1985), the pulsation and rotation axes are aligned (or there are radial $\ell = 0$ modes), but the ratio of flux to radius variations varies over the surface because of differences in the flux and temperature caused by spots associated with the magnetic field. The observed radial velocity (RV) amplitude is then constant, but the photometric amplitude modulates as the star rotates. Therefore, the two models can be distinguished by RV observations. Matthews et al. (1988) found RV amplitude variation in HR 1217 which favoured the oblique pulsator model, but this star is multiperiodic, so the observed variation could have been caused by beating among pulsation frequencies. Kurtz et al. (1994a) proposed that the two models could easily be distinguished by RV measurements of HR 3831. This roAp star has one dominant pulsation mode with a period of 11.7 min, has a large photometric amplitude modulation including a phase reversal (Kurtz et al. 1994a, 1997) and is bright enough for accurate RV measurements ($V = 6.25$).

We obtained time-series spectroscopy of HR 3831 over one week in 1997 March. Preliminary analysis of the Hα RV measurements was presented by Baldry, Kurtz & Bedding (1998b; hereafter BKB) and showed that the radial velocity amplitude is modulated with the rotation of the star. A frequency analysis showed a frequency triplet with the same spacing and amplitude ratios as contemporaneous photometric observations. This is expected in the oblique pulsator model, and is in clear disagreement with the prediction of the spotted pulsator model.

In this paper we describe more detailed analyses of our HR 3831 spectra using some of the techniques that were used by Baldry et al. (1998a, 1999; hereafter B98, B99) to study α Cir. These include cross-correlations of different wavelength regions, line shifts of the Hα bisector and intensity measurements across the Hα line. While the oblique pulsator explains most of the observed rotational modulations, aspects of the spotted pulsator model and perturbed *m*-modes may also be required to explain our results.

1.1 Basic data for HR 3831

HR 3831 (IM Vel, HD 83368, HIP 47145) has a binary companion with $V = 9.09$ with a separation of 3.29 arcsec. The visual magnitude of HR 3831 is often quoted as $V = 6.17$, but this is from the combined flux measurement (see Kurtz et al. 1994a). Using the correct value of $V = 6.25$, the *Hipparcos* distance of 72.5 ± 4 pc (ESA 1997), an effective temperature of 8000 ± 200 K (Kurtz et al. 1994a) and a bolometric correction of -0.13 (Schmidt-Kaler 1982), we obtain $L = 13.4 \pm 1.5 L_\odot$ and $R = 1.9 \pm 0.2\,R_\odot$.[2]

The oscillation spectrum of HR 3831 has a well-known frequency septuplet around 1428 μHz, plus frequency multiplets at the harmonics (Kurtz et al. 1997). However, there are just four frequencies which have photometric amplitudes above 0.3 mmag (Johnson *B*) and that are detectable in our data. These include a triplet around the principal mode ($\nu_{-1} = 1423.95$ μHz, $\nu_0 = 1428.01$ μHz, $\nu_{+1} = 1432.07$ μHz) and the first harmonic ($2\nu_0 = 2856.02$ μHz).

The splitting of the triplet ($\nu_{\rm rot} = 4.06$ μHz) gives the rotation period $P_{\rm rot} = 2.851\,976$ d, assuming that the oblique pulsator model is correct. Unlike the triplet in α Cir (Kurtz et al. 1994b), where the amplitudes of the two side-lobes are about 10 per cent of the principal amplitude, the amplitudes of ν_{-1} and ν_{+1} are larger than the amplitude of the central frequency. This means that during the rotation cycle of HR 3831, the amplitude measured at ν_0 goes through two maxima with two phase reversals. In terms of the oblique pulsator model, the star pulsates in an $\ell = 1$ dipole mode which is sufficiently oblique to the rotation axis that we see first one pole and then the other as the star rotates.

Kurtz, Shibahashi & Goode (1990; Kurtz 1990) described a generalized oblique pulsator model in which the effects of both the magnetic field and rotation were taken into account (see also Dziembowski & Goode 1985, 1986). In this model, the perturbation to the eigenfrequencies of the star by the magnetic field dominates, leading to the conclusion that the pulsation axis is locked to the magnetic axis. Two parameters related to the amplitude ratios in the frequency triplet were defined:

$$P_1 = \frac{A_{+1} + A_{-1}}{A_0} = \tan i \tan \beta, \tag{2}$$

where i is the inclination of the rotation axis to the line of sight, and β is the angle between the rotation axis and the pulsation axis; and

$$P_2 = \frac{A_{+1} - A_{-1}}{A_{+1} + A_{-1}} = \frac{C_{n\ell}\,\nu_{\rm rot}}{\nu_1^{(1)\rm mag} - \nu_0^{(1)\rm mag}}, \tag{3}$$

where the perturbation to the eigenfrequencies (by the magnetic field) depends on $|m|$ such that $\nu = \nu^{(0)} + \nu_{|m|}^{(1)\rm mag}$. From the measured photometric amplitudes for HR 3831 covering 1993 to 1996 (Kurtz et al. 1997), we derive $P_1 = 8.6 \pm 0.2$ and $P_2 = -0.097 \pm 0.004$.

2 OBSERVATIONS

2.1 Spectroscopy

We obtained 1400 intermediate-resolution spectra of HR 3831 using the coudé spectrograph on the 74-inch telescope at Mt. Stromlo Observatory (MSO), Australia. A log of the observations is shown in Table 1. The wavelength region from 6100 to 7100 Å was observed with a resolution of about 1.5 Å and a dispersion of 0.49 Å pixel^{-1}. The average number of photon Å^{-1} in each spectrum was 270 000, with a minimum of 60 000. The exposure time was 100 s, with an over-head between exposures of 20 s.

All CCD images were reduced to spectra using the same procedures that were used on the Mt. Stromlo data for B98.

Table 1. Log of the spectroscopic observations of HR 3831.

UT date	No. of hours	No. of spectra	Julian dates −245 0000
1997 Mar 10	1.37	26	517.88–517.94
1997 Mar 10	3.61	38	518.12–518.27
1997 Mar 11	10.03	203	518.88–519.29
1997 Mar 12	9.59	285	519.88–520.28
1997 Mar 13	2.22	59	520.88–520.97
1997 Mar 13	1.10	33	521.27–521.32
1997 Mar 14	10.57	319	521.87–522.31
1997 Mar 15	10.40	262	522.88–523.31
1997 Mar 16	9.40	158	523.87–524.27
1997 Mar 17	0.53	17	524.87–524.90

[2] In some papers (including BKB), the radius of HR 3831 is incorrectly quoted as $2.9\,R_\odot$. This may be the result of the propagation of a typographical error.

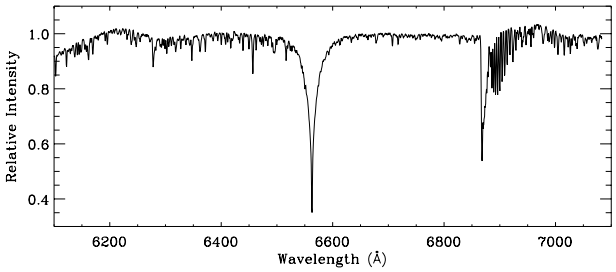

Figure 1. The template spectrum of HR 3831.

Table 2. Photometric (Johnson *B*) amplitudes and phases[a] of the frequency triplet (BKB). From this data, $P_1 = 6.9 \pm 0.7$ and $P_2 = -0.07 \pm 0.02$.

frequency (μHz)	amplitude (mmag)	phase[a] (radians)
1423.95	1.91 ± 0.05	1.00 ± 0.03
1428.01	0.52 ± 0.05	-1.16 ± 0.10
1432.07	1.66 ± 0.05	1.03 ± 0.03

[a] The phases are shifted compared to the those given in BKB because of a different phase reference point (see Section 3).

Several observables were defined from the spectrum (velocities, intensities, bisector measurements), to produce a time-series of measurements for each observable. For use in various measurements, a template spectrum was defined from 25 high-quality spectra (Fig. 1).

2.2 Photometry

For the last five years, astronomers at the South African Astronomical Observatory (SAAO) and the University of Cape Town (UCT) have been monitoring the oscillations in HR 3831 using high-speed photometry (Kurtz et al. 1997). For BKB, a subset of their data was selected which is centred on the time of the spectroscopic observations. These data were obtained on 26 nights (one hour of high-speed photometry per night) spanning the dates JD 245 0402 to 245 0618.

The photometry was analysed to find the amplitudes and phases of the frequency triplet (see Table 2) in order to compare with the spectroscopic results. The amplitudes of the triplet are within 2σ of the amplitudes from Kurtz et al. (1997). For further details, in particular showing the pulsation amplitude and phase as a function of rotation phase, see BKB.

3 TIME-SERIES ANALYSIS

To illustrate the various methods of analysing the time series for each spectroscopic observable, we look at an observable which has a high signal-to-noise ratio in the oscillation spectrum. This observable, called $R_{\rm cw}$, is a ratio of the Hα core to wing intensity. In particular, we divided the intensity in a filter with full width at half-maximum (FWHM) $\sim$4 Å by that in a filter with FWHM $\sim$31 Å. This is similar to the $R_{\rm cw}$ measurements used for B99 and BKB but using slightly narrower filters.

Each time series from the spectroscopic measurements was high-pass filtered and a few outlying points were removed. The

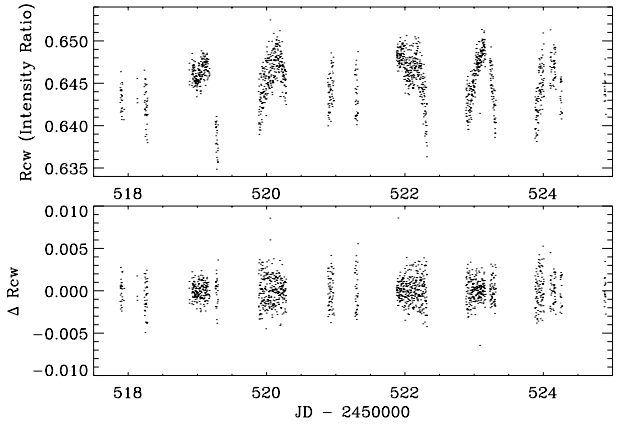

Figure 2. $R_{\rm cw}$ time series before and after high-pass filtering.

$R_{\rm cw}$ time series before and after high-pass filtering is shown in Fig. 2. There is a variation in the raw data of about 1 per cent during the night. This is possibly a result of varying contamination of the HR 3831 spectrum from its binary companion. As the pair of stars rotates in the coudé focal plane, there will be less contamination when the stars line up perpendicular to the slit and more contamination when the stars line up along the slit. Alternatively, the variation could be the result of instrumental effects that are a function of the elevation of the telescope. In either case, the change in the measured oscillation amplitude will be of the order of 1 per cent over the night. This is not significant for our results, especially since there is no obvious systematic effect as a function of the rotation phase of HR 3831.

Next, a simultaneous fit of the frequency triplet and the first harmonic was made to the high-pass filtered data, using a weighted least-squares fitting routine. The amplitudes and phases were fitted, using the well-known frequencies (see Section 1.1), by the function $A \sin[2\pi\nu(t - t_0) + \phi]$ where $t_0 =$ JD 245 0522.51746. Our phase reference point t_0 is equal to the reference point of Kurtz et al. (1997) plus 775 times $P_{\rm rot}$. This maintains the same relationship between the phases of the frequency triplet. The fit of the frequency triplet to the $R_{\rm cw}$ data is shown in Table 3 (the results for three sets of filters are shown).

The $R_{\rm cw}$ oscillation amplitude spectrum is shown in Figs 3–4. Fig. 4 shows that the frequency triplet is resolved, but with some aliasing or power shifting between the frequencies, as can be seen from the spectral window. The amplitude of the spectral window at $\pm\nu_{\rm rot}$ and at $\pm 2\nu_{\rm rot}$ is about 20 per cent. Also, the simultaneous fit gives amplitudes in ppm of 1330, 180 and 1140 for the triplet, whereas the amplitudes in the oscillation spectrum are 1100, 560 and 890 (note that ratio between A_{-1} and A_{+1} is about the same).

Another way to consider the aliasing is that the data have incomplete and biased sampling of the rotation phase of HR 3831. A good diagnostic of the data is to plot the amplitude and phase of the pulsation (at ν_0) as a function of rotation phase. This is better for interpretation assuming that there is one mode, which is amplitude modulated, rather than three distinct modes. We divided the data into 20 separate time intervals between 0.5 and 3.6 h long and including between 17 and 107 spectra. For each time interval, the amplitude and phase were measured at 1428.01 μHz. The $R_{\rm cw}$ results are shown in Fig. 5. The two lines represent different fits to the data.

(i) The dashed line represents a modulation using the amplitudes and phases of the $R_{\rm cw}$ frequency triplet (from

Table 3. R_{cw} amplitudes and phases of the frequency triplet in HR 3831. The observable R_{cw} is the ratio between the mean intensity in a narrow filter with FWHM $F1$ and in a filter with FWHM $F2$ centred on Hα. For the three observables in this table, the average values are about 0.65 (see Fig. 2 for the raw data in the second case).

$F1$ (Å)	$F2$ (Å)	frequency (μHz)	amplitude (ppm)	phase (radians)	P_1	P_2
		1423.95	1340 ± 46	-0.82 ± 0.03		
2.9	23.5	1428.01	172 ± 45	-1.28 ± 0.27	15.8 ± 4.7	$+0.02 \pm 0.02$
		1432.07	1386 ± 46	-0.78 ± 0.03		
		1423.95	1334 ± 41	-0.71 ± 0.03		
3.9	31.4	1428.01	177 ± 40	-1.58 ± 0.23	14.0 ± 3.5	-0.08 ± 0.02
		1432.07	1139 ± 41	-0.78 ± 0.04		
		1423.95	1107 ± 41	-0.64 ± 0.04		
5.9[a]	45.1[a]	1428.01	163 ± 41	-1.70 ± 0.25	12.4 ± 3.4	-0.10 ± 0.03
		1432.07	913 ± 41	-0.78 ± 0.05		

[a] This set of R_{cw} results uses the same filters as the R_{cw} results published in BKB. The results are slightly different because of a different weighting in the least-squares fitting routine, and there is also a change in phase reference point.

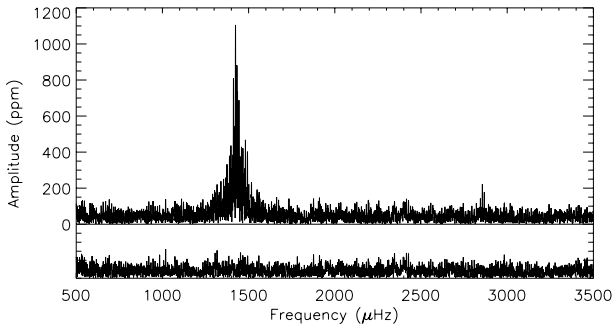

Figure 3. R_{cw} amplitude spectrum. The lower panel is the pre-whitened amplitude spectrum after subtracting a simultaneous fit of the frequency triplet and the harmonic.

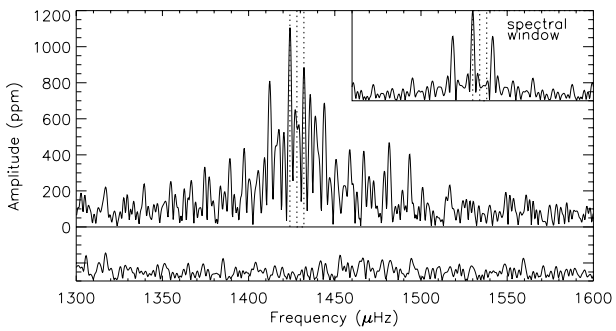

Figure 4. Close-up of Fig. 3, with the dotted lines showing the frequencies of the triplet. The inset shows the amplitude spectrum of the window function on the same frequency scale, with the dotted lines having the same spacing as in the triplet.

Table 3), which are from a six-parameter fit to the complete time series. In other words, it shows the beating effect of the three close frequencies (ν_{-1}, ν_0, ν_{+1}). The good agreement between the modulation in amplitude and phase from the separate time intervals and the modulation from the frequency triplet supports the accuracy of the simultaneous fit to the triplet.

(ii) The dotted line represents a fit which is obtained by scaling and phase shifting from the *photometric* analysis of the triplet (from Table 2). In effect, this is a two-parameter fit to the

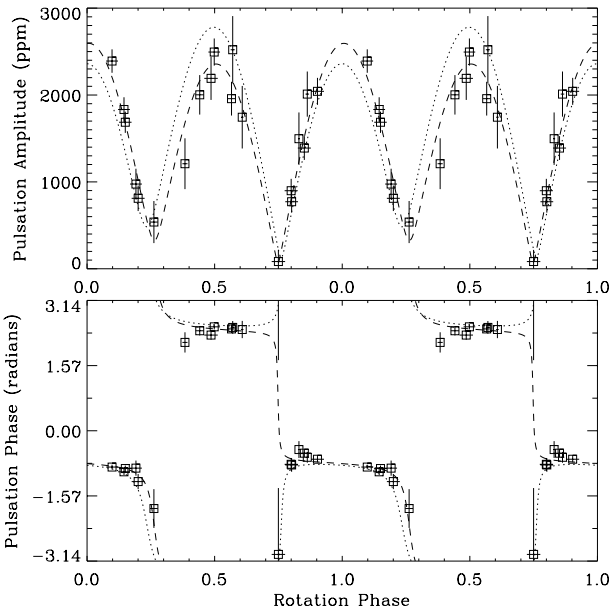

Figure 5. R_{cw} amplitude and phase of the central frequency as a function of rotation phase. The squares represent the data divided into 20 separate time intervals between 0.5 and 3.6 h long. The vertical lines are error bars, while the horizontal lines show the length of the time intervals. The dashed line represents a fit based on the measurement of the frequency triplet from the complete time series, and the dotted line represents a fit which is scaled and phase shifted from the photometric frequency triplet. See Section 3 for further details of the time-series analysis. Note that the data are plotted twice.

amplitudes and phases of the separate time intervals. The shape of the amplitude and phase modulation is the same as the beating effect of the photometric triplet, while one parameter is the scaling of the amplitude and the other parameter is the shift of the pulsation phase. In this case, a reasonable fit is obtained to the R_{cw} data.

In conclusion, we have clearly detected the triplet in the equivalent width of Hα (using R_{cw}) with the amplitudes of the three components in about the same ratio as seen in photometry. The R_{cw} measurement, as in α Cir (B99), provides a high signal-to-noise ratio spectral measurement of the pulsation.

4 VELOCITIES OF WAVELENGTH BANDS

In this section, we look at the velocity amplitude and phase of different wavelength bands using a cross-correlation technique. The reduction method is the same as that used on α Cir, with a telluric band used as a velocity fiducial (sections 3.2–3.3 of B98). The spectrum of HR 3831 was divided into 90 bands, most having the same wavelength range as shown in table 3 of B98, the difference being that the spectrum of HR 3831 was taken from 6100 to 7100 Å, which is 100 Å higher than the range used in the α Cir analysis. The results for 10 selected bands are shown in Table 4.

4.1 Hα velocity

First, we look again at the Hα velocity (previously analysed for BKB), as measured using the cross-correlation of band no. 87 (6545–6578 Å). This band has a good signal-to-noise ratio and should not be significantly affected by blending. The Hα velocity amplitude and phase as a function of rotation phase are shown in Fig. 6. There is excellent agreement between the fit based on the measurement of the frequency triplet (Table 4) and the fit scaled and phase-shifted from the photometric data (Table 2). This rules out the spotted pulsator model. In this model, the pulsation velocity amplitude and phase should be

Table 4. Velocity amplitude and phases for selected wavelength bands using a cross-correlation technique. The bands selected were those having a combined signal-to-noise[a] ratio of greater than nine for the frequency triplet, except that only one band across the Hα line is included (band no. 87). A telluric band from 6864 to 6881 Å is used as a velocity reference (band no. 80).

band[b] range (Å)	frequency (μHz)	amplitude ($m\,s^{-1}$)	phase (radians)	P_1[c]	P_2	Figure
no. 13	1423.95	377 ± 51	0.82 ± 0.13			
	1428.01	92 ± 50	-0.67 ± 0.57	–	-0.18 ± 0.12	–
6140.6–6150.9	1432.07	260 ± 51	0.89 ± 0.20			
no. 14	1423.95	524 ± 61	2.45 ± 0.12			
	1428.01	26 ± 61	–	–	-0.32 ± 0.12	–
6152.9–6164.6	1432.07	273 ± 61	2.41 ± 0.23			
no. 18	1423.95	1108 ± 69	0.07 ± 0.06			
	1428.01	228 ± 68	-1.33 ± 0.30	6.6 ± 2.3	-0.48 ± 0.07	9
6194.0–6197.5	1432.07	392 ± 69	0.09 ± 0.18			
no. 33	1423.95	1140 ± 62	0.54 ± 0.05			
	1428.01	222 ± 62	-0.96 ± 0.28	7.6 ± 2.4	-0.34 ± 0.05	–
6325.8–6333.2	1432.07	556 ± 62	0.46 ± 0.11			
no. 42	1423.95	600 ± 64	1.26 ± 0.11			
	1428.01	118 ± 64	-0.77 ± 0.57	–	-0.13 ± 0.09	–
6414.0–6422.9	1432.07	458 ± 64	0.70 ± 0.14			
no. 54	1423.95	348 ± 60	1.64 ± 0.17			
	1428.01	88 ± 60	-0.44 ± 0.75	–	$+0.10 \pm 0.11$	–
6521.8–6528.2	1432.07	423 ± 60	1.62 ± 0.14			
no. 58	1423.95	1378 ± 132	2.36 ± 0.10			
	1428.01	131 ± 131	-0.47 ± 1.49	–	-0.60 ± 0.13	–
6596.3–6607.1	1432.07	346 ± 132	2.83 ± 0.39			
no. 81[d]	1423.95	63 ± 12	-2.59 ± 0.19			
	1428.01	16 ± 12	1.99 ± 0.80	–	$+0.03 \pm 0.13$	–
6881.5–6901.6	1432.07	68 ± 12	2.54 ± 0.18			
no. 87[e]	1423.95	343 ± 22	1.58 ± 0.06			
	1428.01	94 ± 22	-0.81 ± 0.24	6.9 ± 1.8	-0.05 ± 0.05	6
6545.4–6578.2	1432.07	309 ± 22	1.42 ± 0.07			
no. 90[f]	1423.95	743 ± 87	0.95 ± 0.12			
	1428.01	116 ± 87	-1.15 ± 0.84	–	-0.35 ± 0.12	–
7070.2–7079.5	1432.07	357 ± 87	1.28 ± 0.25			

[a] The rms noise is about 1.38 times the formal 1σ uncertainty on the amplitude measurements.
[b] The band number relates to the bands used in B98.
[c] Only the bands where the central amplitude is higher than 2σ are included. For the other bands, the uncertainty in this parameter is large and significantly non-Gaussian.
[d] This band contains a significant number of telluric lines, see discussion in section 5.1 of B98.
[e] This band represents the velocity of the Hα line. These results are different from those published in BKB because the band is wider and the telluric band used as a reference is different.
[f] This is a new band not included in B98.

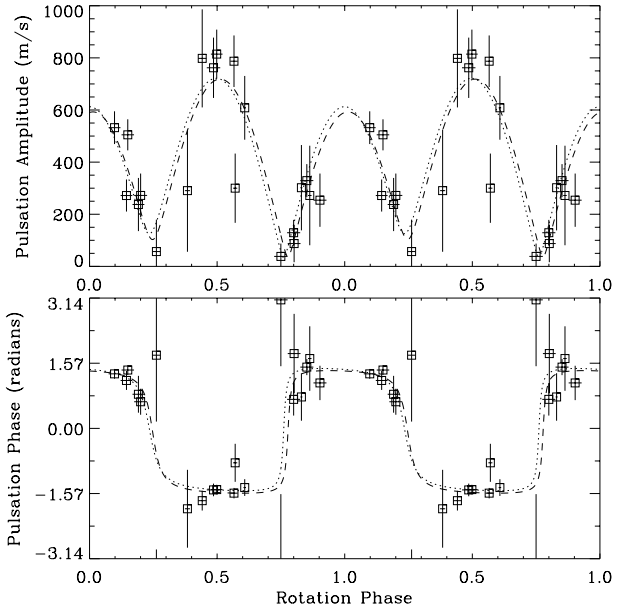

Figure 6. Hα velocity amplitude and phase of the central frequency as a function of rotation phase (band no. 87). Line styles have the same meanings as in Fig. 5. There is excellent agreement between the two fits, which rules out the spotted pulsator model.

constant during the rotation of the star, which is clearly not the case.

The excellent agreement between the Hα velocity and photometry, in terms of the relative modulation as a function of rotation phase, is reflected in the fact that the parameters P_1 and P_2 are nearly the same between the two time series (compare Table 2 with band 87 from Table 4). Within the oblique pulsator model, these parameters are expected to be the same for different observables (see Section 1.1). If the frequency triplet were caused by three different modes, then the ratios between the amplitudes of the modes (quantified by P_1 and P_2) would be expected to vary depending on the observable. Therefore, this agreement between the Hα velocity and photometry argues in favour of the oblique pulsator model rather than for different modes.

However, this is a weak argument because the amplitude ratios could be nearly the same even in the case of different modes. The main arguments against different modes come from the years of photometric analysis of HR 3831 (e.g.: Kurtz et al. 1990, 1993, 1994a, 1997): (i) the frequency splitting is exactly or nearly exactly the rotation frequency (see Section 1), and (ii) the ratios between the amplitudes of the frequency triplet have remained nearly constant over time. For these reasons, it is considered unlikely that the observed frequency triplet in HR 3831 is caused by different modes, in particular rotationally perturbed *m*-modes.

In BKB, a possible rotational phase lag was noted, between the radial velocity (RV) amplitude maximum and the photometric amplitude maximum, of about 0.06 rotation cycles. However, from the results shown in Fig. 6, the RV maximum and photometric maximum are within 0.02 rotation cycles of each other. The change from the earlier results arises from the use of a different telluric reference wavelength region. In BKB, a large region from 6865 to 6931 Å was used, which included bands 80, 81 and 82, in order to maximize the signal-to-noise ratio. In this paper, we find a significant signal arising from the wavelength region of band 81 (see Table 4) and this is likely to be the cause of the phase lag noted in BKB. Band 80 alone is used as the telluric

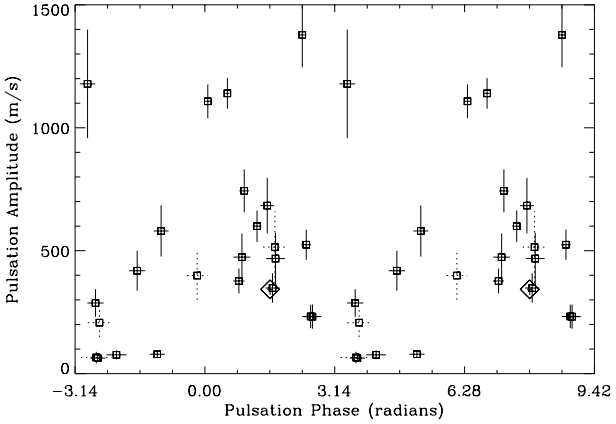

Figure 7. Velocity amplitudes and phases measured at the frequency ν_{-1} in HR 3831 for different wavelength bands. Bands with S/N greater than 3 are plotted with solid lines, those with lower S/N have dotted lines. The same 25 bands are plotted in this figure and in Fig. 8, chosen so that the *combined* S/N is greater than 5. Only one band across Hα is included and is shown using a diamond. Note that the data are plotted twice for clarity.

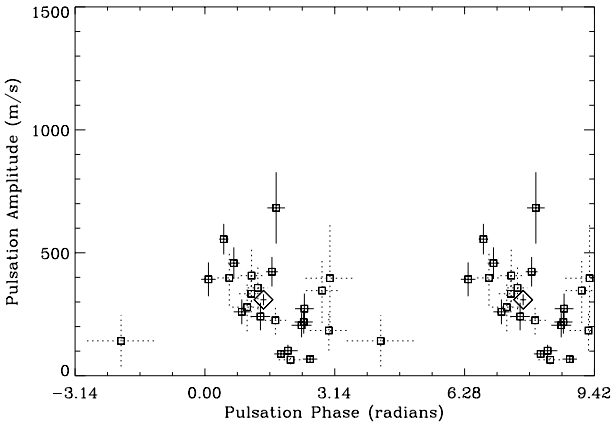

Figure 8. Same as Fig 7, but for the frequency ν_{+1}.

reference band in this paper because it has the lowest percentage (about 2 per cent) of absorption that is attributable to lines from the star (see discussion in section 5.1 of B98). To summarize, the Hα RV amplitude is better represented by the results in this paper, whereas the results in BKB are slightly contaminated by metal lines around band 81.

4.2 Metal lines

The velocity amplitude and phase in HR 3831 varied significantly between different wavelength bands, as was seen in α Cir (B98). Figs 7–8 show the amplitude versus pulsation phase in HR 3831 for the 24 metal bands with the highest signal-to-noise ratios (plus one band across Hα). The results measured at the frequencies ν_{-1} and ν_{+1} are plotted separately, while the amplitude and phase of ν_0 are not plotted because the signal-to-noise ratio (S/N) is significantly lower at this frequency. There are two aspects to the results which we will consider: the modulation of the measured pulsation with rotation and the variation of the amplitude and phase between different wavelength bands. The first is characterized by the difference in amplitude and phase between ν_{-1} and ν_{+1}.

4.2.1 Rotational modulation

There is a significant difference between the results for ν_{-1} (Fig. 7) and ν_{+1} (Fig. 8). First, the amplitudes vary between 0 and 1500 m s^{-1} for ν_{-1}, whereas the amplitudes for ν_{+1} are all below 800 m s^{-1}. Secondly, the phases range across 2π for ν_{-1}, while the phases for ν_{+1} range between 0 and π except for one low S/N band. This is not as expected from the oblique pulsator model. In this model, for each band, the phase of ν_{-1} and ν_{+1} should be the same and the amplitudes should be nearly the same ($A_{+1} \approx 0.87 \times A_{-1}$ from Table 2). Therefore, these results suggest that the two frequencies measured are separate modes, rather than rotational 'side lobes' of one principal mode. However, there is strong evidence for the oblique pulsator model as described in Section 4.1. Therefore, we need to consider another explanation within the framework of the oblique pulsator model. We first look at some selected bands, in terms of their modulation of amplitude and phase with rotation.

Recall that the oblique pulsator model involves parameters P_1 and P_2 (equations 2 and 3). All the measured spectroscopic observables in this paper produce values for P_1 that are within 3σ of the photometric value. However, there are large uncertainties in this parameter because it depends critically on the amplitude measured at ν_0, which is typically less than two or three times the noise level in our data.

The parameter P_2 can be measured with higher accuracy since it does not depend on the small central amplitude, and we find that it does vary significantly between different observables. From the measured velocity amplitudes, there are three spectral bands (18, 33 and 58) that have values of P_2 that are formally 4–5σ different from the photometric value (see Table 4). To test whether this is a significant change or just a product of aliasing, we looked at the modulation in velocity amplitude and phase as a function of rotation phase. Fig. 9 shows this modulation for band 18. While the amplitude modulation could be fitted reasonably well by scaling from the photometry (dotted line), the discrepancy is obvious with the phase modulation. There is a noticeable pulsation phase change from rotation phase 0.8 through 1.0 to 0.2, while the photometric phase is nearly constant. Similar effects are evident from the other bands, 33 and 58, for which the P_2 value is significantly different from the photometric value.

Fig. 10 shows a plot of P_2 versus the average amplitude of frequencies ν_{-1} and ν_{+1}. There is a noticeable tendency for higher amplitude bands to have lower values of P_2. This could be related to the line-formation depth or position on the surface (i.e., spots). Alternatively, a systematic effect (e.g., blending) could be increasing the measured amplitude at ν_{-1} only causing an increase in average amplitude and a decrease in P_2.

As well as the parameters P_1 and P_2, which relate the amplitudes of the frequency triplet, there are also phase differences between the frequencies. For many bands, there is significant difference between the phases measured at ν_{-1} and ν_{+1}. In our measurements, the equality of phase ϕ_{-1} and ϕ_{+1} means that the amplitude maxima occur at rotation phases 0.0 and 0.5 with phase jumps in between. Therefore, any phase difference, $\phi_d = \phi_{+1} - \phi_{-1}$, implies that there is a shift of the amplitude maxima. For example, there is a small shift in the amplitude maxima of band 42 ($\phi_d = -0.56 \pm 0.18$) and larger shifts, but with lower S/N in the amplitude spectra, of bands 48 ($\phi_d = -2.29 \pm 0.31$) and 82 ($\phi_d = 2.99 \pm 0.25$). Fig. 11 shows the modulation for band 48. Note that the pulsation-phase jumps occur out of (rotation) phase with the photometric pulsation-phase jumps.

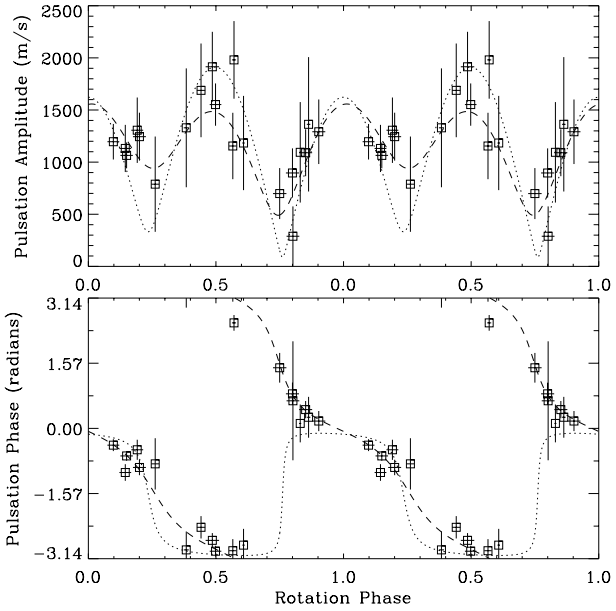

Figure 9. Velocity amplitude and phase of band no. 18 as a function of rotation phase. Line styles have the same meanings as in Fig 5.

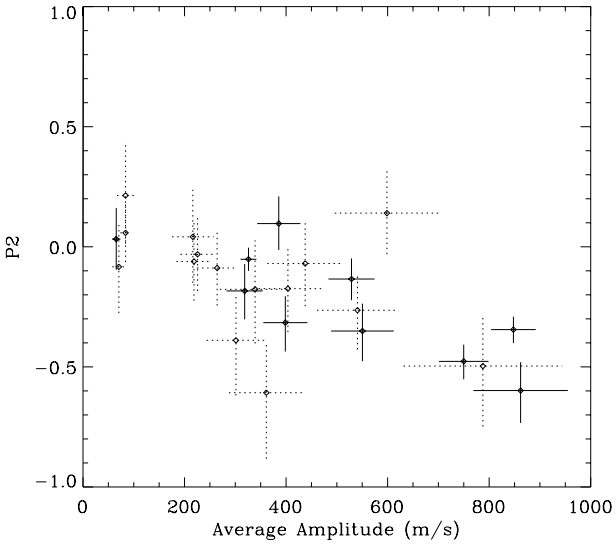

Figure 10. Plot of the parameter P_2 versus the average amplitude of frequencies ν_{-1} and ν_{+1}, with 1σ error bars, for the 25 bands that are shown in Figs 7 and 8. Points with solid lines represent the higher S/N bands given in Table 4. Note that the four lowest amplitude bands in this figure are contaminated by telluric lines. For these bands, the cross-correlation measurement of the velocity amplitude is reduced compared to an uncontaminated band (with equivalent stellar behaviour).

These results are not sufficient evidence to discard the oblique pulsator model, because they could be explained by variations in the ratios between the metal lines in the bands, arising from spots, as the star rotates. Alternatively, there is a possibility that there is an actual change in the pulsation phase and amplitude (as opposed to a pseudo-change caused by a variation in blending) associated with spots on the star. So while the spotted pulsator model is ruled out in its original form, spots may be having an influence on the pulsation.

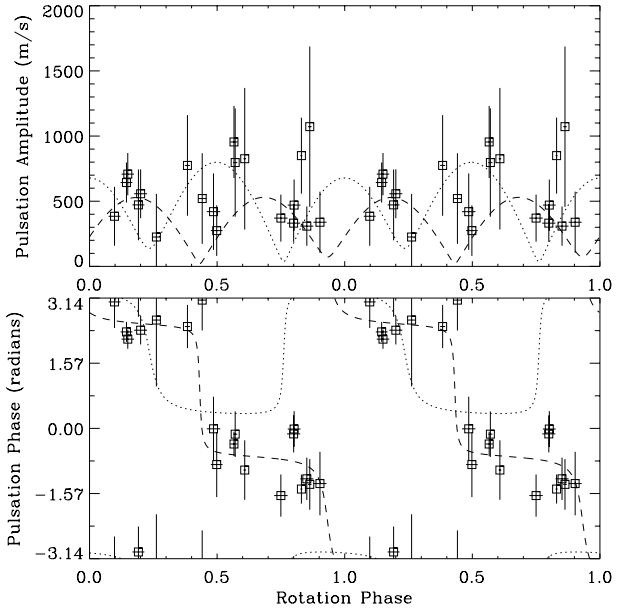

Figure 11. Velocity amplitude and phase of band no. 48 as a function of rotation phase. Line styles have the same meanings as in Fig. 5.

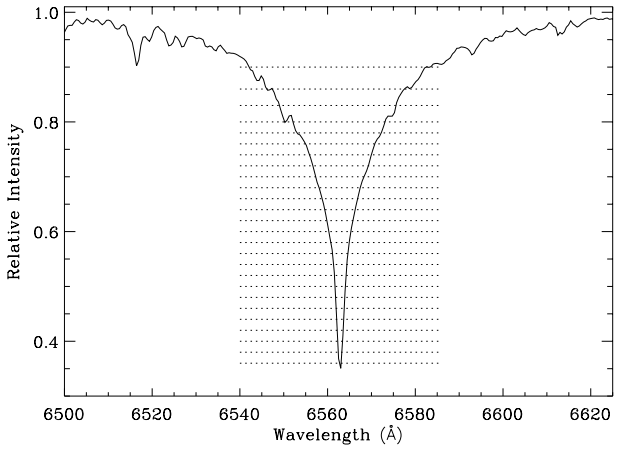

Figure 12. The Hα line in HR 3831. The dotted lines divide the 25 contiguous sections used in the bisector velocity and width analysis (Section 5).

4.2.2 *Amplitude and phase variations between bands*

In B98, it was suggested that the amplitude and phase variations between wavelength bands in α Cir could be explained by a radial node in the atmosphere. We see amplitude and phase variations in HR 3831 that are somewhat similar in the case of ν_{-1} (Fig. 7), and with smaller but still significant variations in the case of ν_{+1} (Fig. 8). However, there is no obvious division between two sets of bands that are pulsating in antiphase with each other, as was seen in α Cir (B98). If these HR 3831 results represent true velocity amplitudes and phases at various depths in the atmosphere, then an explanation that includes running waves is necessary. Alternative explanations could involve spots on the surface or blending, which causes the measured phase to deviate from the true velocity phase (for further discussion see Section 6.1.2, below).

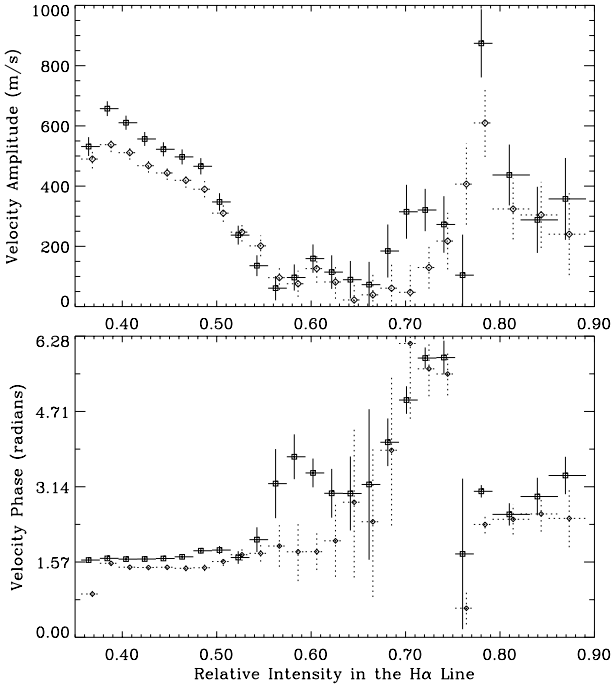

Figure 13. Amplitudes and phases of the pulsation for the bisector velocity at different heights in the Hα line. Squares with solid lines represent ν_{-1} and diamonds with dotted lines represent ν_{+1}. For each measurement, the vertical line is an error bar while the horizontal line shows the extent of the section in the Hα line.

5 Hα PROFILE VARIATIONS

In α Cir we found intriguing behaviour in the Hα line that implied the existence of a radial node in the atmosphere (B99). We now describe a similar analysis for HR 3831. The Hα line in each spectrum was divided into 25 contiguous horizontal sections, between relative intensities 0.35 and 0.9 (Fig. 12). For each section, a bisector velocity (average position of the two sides) and a width were calculated. For the velocity measurements, a telluric band (no. 80) was used as a fiducial.

5.1 Bisector velocities

The velocity amplitude and phase of the pulsation as a function of relative intensity in the Hα line are shown in Fig. 13, with measurements at frequencies ν_{-1} and ν_{+1}. The amplitudes and phases are in good agreement between the two frequencies, which means that the shape of the rotational modulation is similar for each velocity measurement. Fig. 14 shows the rotational modulation from the velocity at a height of 0.40. It is similar to the modulation from the cross-correlation velocity of Hα (Fig. 6), but with about twice the amplitude. This is expected because the cross-correlation velocity is a weighted average of the bisector velocities and the velocity amplitude at 0.40 is higher than average.

The variation in amplitude and phase as a function of relative intensity (Fig. 13) is similar to that seen in α Cir, particularly the drop in amplitude between heights 0.4 and 0.6 (a comparison is shown in Fig. 15). However, assuming that the bisector line-shift represents the velocity at different heights in the atmosphere, we expect to see less relative variation in the bisector-velocity

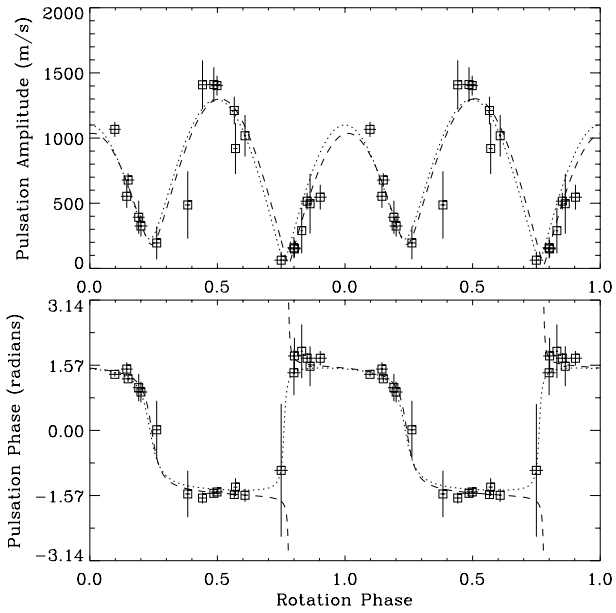

Figure 14. Velocity amplitude and phase of the Hα bisector at height 0.40 as a function of rotation phase. Line styles have the same meanings as in Fig. 5.

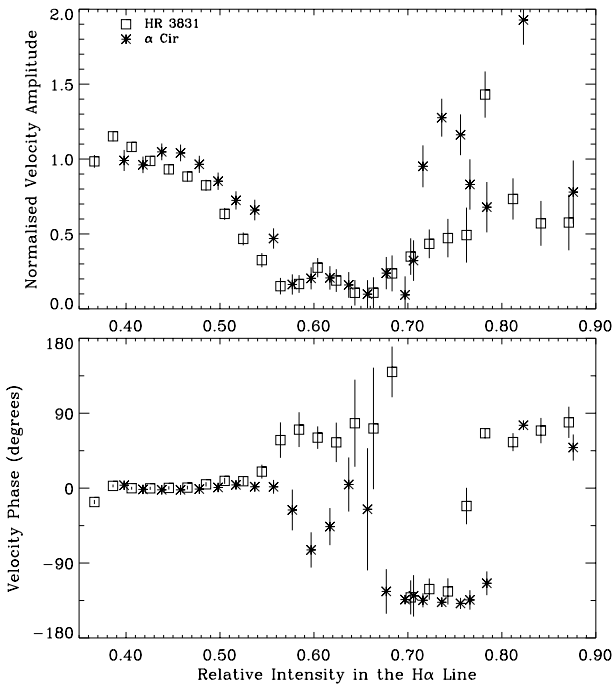

Figure 15. Comparison of the Hα bisector variations between HR 3831 and α Cir. This figure is essentially a normalized overplot of Fig. 13 of this paper and fig. 7 of B98, except that for HR 3831 the measurements for ν_{-1} and ν_{+1} were averaged and for α Cir the Mt. Stromlo and La Silla data were combined. Additionally, the amplitudes were normalized by dividing by an average taken between heights 0.40 and 0.45 (519 m s^{-1} for HR 3831 and 267 m s^{-1} for α Cir) and the phases were shifted.

amplitude in HR 3831 than in α Cir. This is because the separation between radial nodes in the atmosphere is larger in HR 3831 as a result of the fact that it pulsates at a lower frequency and that the two stars have similar fundamental properties.

Why are the behaviours of α Cir and HR 3831 so similar? Two possible explanations are: (i) the Hα line-forming region in HR 3831 is more extended than in α Cir and coincidently the Hα bisector behaves in a similar way; (ii) the assumption that the bisector represents velocities at different heights is incorrect.

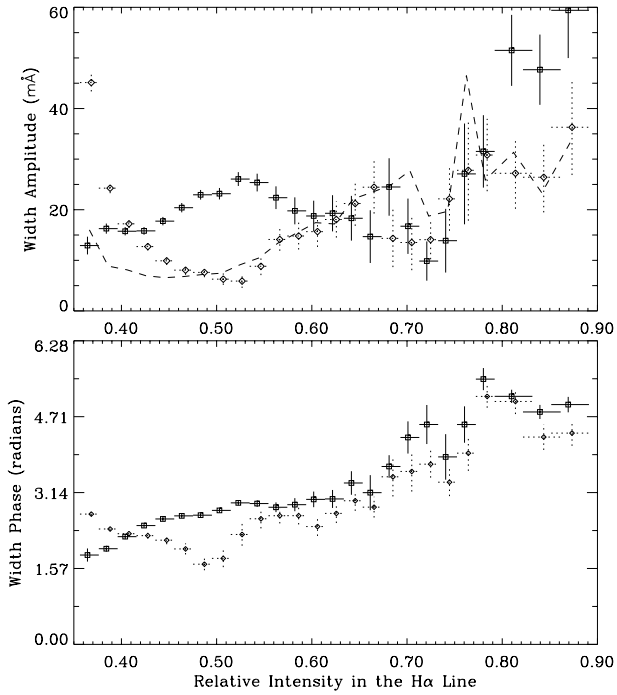

Figure 16. Amplitudes and phases of the pulsation for the width at different heights in the Hα line. Points with solid lines represent ν_{-1} and points with dotted lines represent the ν_{+1}. For each measurement, the vertical line is an error bar while the horizontal line shows the extent of the section in the Hα line. The dashed line shows the effect on the width amplitude of an oscillation with an EW amplitude of 1000 ppm, with the profile variation described in section 4.2 of B99. Note that 10 m Å is equivalent to a velocity of 457 m s^{-1} at Hα.

The variation in amplitude and phase is less similar to α Cir above a height of 0.7. For instance, there is a noticeable amplitude peak and phase reversal around 0.73 in the bisector of α Cir which is not evident in HR 3831. The bisector measurements above a height of 0.7 in α Cir are partially affected by blending (section 3.2 of B99). Therefore, some of the differences in the bisector velocity results between the two stars are probably the result of a difference in blending.

To summarize, there is no significant difference in the rotational modulation of the bisector velocity between various heights. For the measurements below a height of 0.7, the relative variation in amplitude and phase is very similar to that observed in α Cir, which is puzzling. At each height, the amplitudes at the two frequencies in HR 3831 are about twice the amplitude of the principal frequency in α Cir.

5.2 Widths

Changes in the width of the Hα line in HR 3831 at various heights are shown in Fig. 16. The width amplitude and phase represent oscillations about a mean width, with measurements at two frequencies. These measurements are related to intensity and equivalent width (EW) measurements, with the line resolved vertically rather than horizontally. The advantage of width measurements is that the width is naturally independent of the

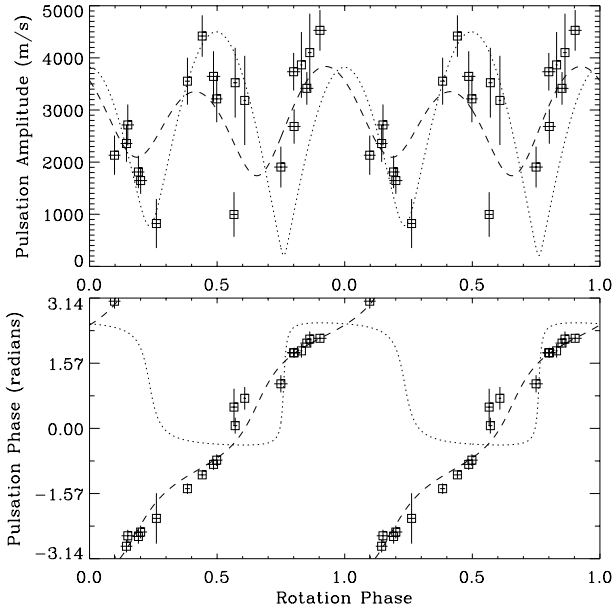

Figure 17. Width amplitude and phase of Hα at height 0.36 as a function of rotation phase. Line styles have the same meanings as in Fig. 5.

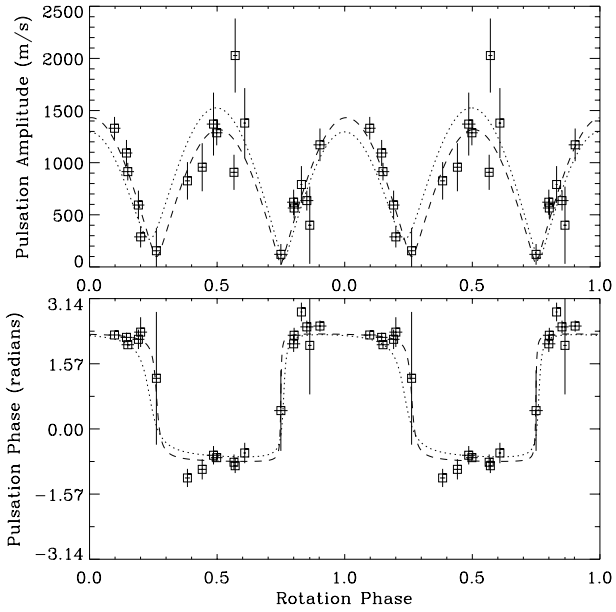

Figure 18. Width amplitude and phase of Hα at height 0.42 as a function of rotation phase. Line styles have the same meanings as in Fig. 5.

bisector velocity, i.e., the width is the difference in position between two sides of a line whereas the velocity is the average position. In order to compare with EW measurements, the dashed line shows the simulated width amplitudes for the profile variation described in section 4.2 of B99 (see also fig. 6 of that paper) with an EW amplitude of 1000 ppm.

The most striking feature of Fig. 16 is the difference in the measurements between the two frequencies. This means that, unlike the case of the bisector velocities, the shape of the rotational modulation is varying between different heights. We show three examples.

(1) Fig. 17 shows the modulation in width amplitude and phase

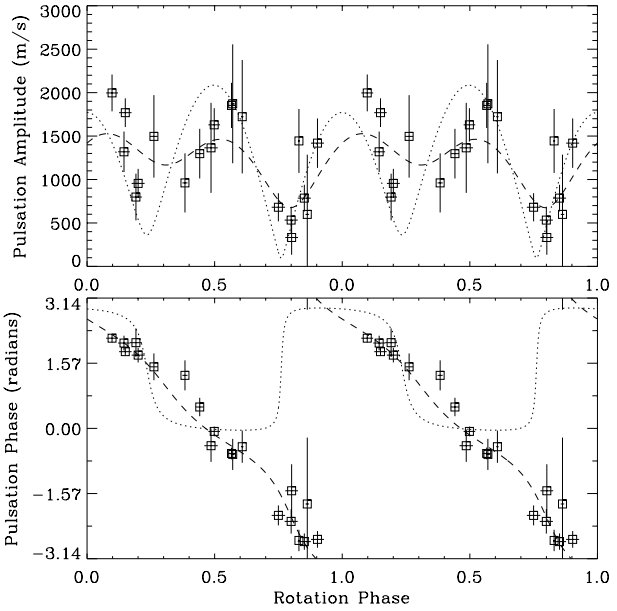

Figure 19. Width amplitude and phase of Hα at height 0.53 as a function of rotation phase. Line styles have the same meanings as in Fig. 5.

at a height of 0.36. The pulsation width phase increases steadily during the rotation and P_2 is large (0.54 ± 0.05).

(2) Fig. 18 shows the modulation at height 0.42. There is good agreement with the fit derived from the photometric triplet and P_2 is -0.03 ± 0.04, which is close to the photometric value.

(3) Fig. 19 shows the modulation at height 0.53. The width phase decreases steadily during the rotation and P_2 is -0.63 ± 0.07.To check the lowest measurement at height 0.36, which is sensitive to intensity changes in the core of the line, we took an intensity measurement using a filter with a FWHM of about 1 Å. This measurement showed a similar rotational modulation, with the parameter $P_2 = 0.33 \pm 0.03$.

Something unexpected is certainly happening here. The Hα width changes at the two extremes, heights 0.36 and 0.53, are in phase at rotation phases around 0.5 and 1.0, but in antiphase at phases around 0.25 and 0.75. At both heights, the relative amplitude modulation (as defined by the dashed line) is less than for other observables.

Looking at Fig. 16, the simple explanation is that we are seeing two modes with different Hα profile variations. An alternative explanation – if HR 3831 is pulsating in an oblique mode – is that, as the star rotates, the profile variation modulates as a result of viewing different aspects of the same mode.

6 DISCUSSION AND CONCLUSIONS

6.1 Velocity amplitudes and phases

6.1.1 Another case: γ Equ

Kanaan & Hatzes (1998) observed radial velocity variations in the roAp star γ Equ. Their observations consisted of high-resolution spectra in the range 5000–6000 Å, covering 3.5 h on 1994 September 13. There are four modes in the range 1330–1430 μHz (Martinez et al. 1996), which are unresolved in that data set. Kanaan & Hatzes fitted a sine curve of fixed frequency (1380 μHz), but variable amplitude and phase, to the velocity

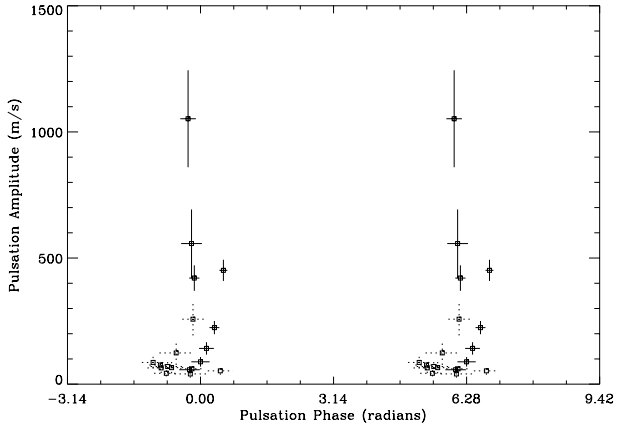

Figure 20. Amplitudes and phases of the pulsation in γ Equ for different metal lines, using results from (Kanaan & Hatzes 1998). Lines with A/σ_a greater than 4 are plotted with solid lines, those with $2.5 < A/\sigma_a < 4$ are plotted with dotted lines. Note that the data are plotted twice for comparison with figs 7 and 10 of B98 and Figs 7 and 8 of this paper.

measurements of each individual line, effectively treating the modes as a single pulsation. They discovered that the velocity amplitude varied significantly from line to line (see B98 and Section 4, above, for similar results on α Cir and HR 3831).

We analysed some of these results on γ Equ, given in table 1 of Kanaan & Hatzes (1998), in order to compare with the results on α Cir and HR 3831. From their table, which lists 70 metal lines, we took the amplitude A ($\mathrm{m\,s^{-1}}$), σ_a ($\mathrm{m\,s^{-1}}$) and the 'time of maximum' (JD). Note that the times of maximum quoted by Kanaan & Hatzes cover several pulsation cycles. We converted the times to phases using the pulsation period of 0.008 387 d, and the phases were shifted so that a weighted mean was approximately zero. The phase uncertainty was taken to be the arcsin (σ_a/A). This phase uncertainty is in good agreement with the σ_b (days) quoted in their table for lines where A/σ_a is greater than 2. Fig. 20 shows amplitude versus phase for the 19 lines with the highest signal-to-noise ratio. The higher amplitude bands, plotted with solid lines, cover a range of 0.8 radians in pulsation phase (-0.26 to $+0.54$ in the figure). This is significantly less than the variation in phase seen in α Cir (fig. 7 of B98) and HR 3831 (Fig. 7), where the bands cover virtually the whole range of phases (2π). Note that the rms noise level in an oscillation spectrum is about $1.38\sigma_a$, therefore, $A/\sigma > 4$ is comparable to $A/\mathrm{noise} > 3$.

The difference between the results for γ Equ (Kanaan & Hatzes) and those for the other two roAp stars, in terms of the variation in phase between different metal bands, could be the result of: (i) wavelength region studied, 5000–6000 versus 6000–7000; (ii) spectrograph resolution, 0.2 versus 1.5 Å; (iii) pulsational characteristics of the stars. Further high-resolution studies of these roAp stars will be able to distinguish among these causes.

6.1.2 *Depth and surface effects*

What are the causes of the velocity amplitude and phase variations, and of the Hα bisector variations?

The main hypothesis is that there is a significant change in pulsation amplitude and phase with geometric depth in the atmosphere of an roAp star, with a radial node of a standing wave situated in the observable atmosphere. Absorption lines are formed at different depths and therefore sample different parts of the standing wave. This can explain a complete range of observed amplitudes plus a phase reversal.

An alternative hypothesis for these variations is that the amplitude and phase of a non-radial pulsation mode will vary over the surface of a star, and that each spectroscopic observable is related to an integral over the surface. Therefore, if the integrals are sufficiently different between observables, the measured amplitude and phase may vary significantly. These variations could be related to limb-darkening and / or spots.

Neither hypothesis can fully explain the range of phases seen in α Cir and HR 3831. Blending effects may cause deviations from the true velocity phases that are in addition to any atmospheric depth and surface effects. The smaller phase variations seen in the high-resolution results of γ Equ lend some support to this. Blending can be considered as blurring the distinction between velocity and temperature changes in a star.

Surface effects would be a good explanation if roAp stars were pulsating in modes with $\ell \geq 3$ because, for these modes, there are several patches on the surface that have alternating phase. However, the frequency triplets in many roAp stars suggest that dipole modes (i.e., $\ell = 1$) are predominant. For these modes, the measured velocity amplitude and phase are not expected to vary significantly between different observables. For example, for a dipole mode with an axis that is aligned near to our line of sight, the pulsation phase will be the same across most of the viewed surface.

The main arguments for depth effects being the principal cause of the amplitude and phase variations are (i) a radial node is plausibly situated in the observable atmosphere (Gautschy, Saio & Harzenmoser 1998), and (ii) the bisector velocity varies with height in the Hα line. In section 3.3 of B99, the possibility of systematic errors causing the bisector velocity variations was discussed. Here, we make a simple calculation to test the accuracy of these velocities below a relative intensity of 0.7 in the line.

For α Cir and HR 3831 (ν_{-1} and ν_{+1}), we averaged the bisector velocity amplitudes below a height of 0.7 (giving half weight to the amplitudes between 0.6 and 0.7) in order to compare with the cross-correlation measurements. This is a plausible estimate for the cross-correlation because the slope of the Hα profile is steep and nearly constant between 0.4 and 0.6, and is less steep above 0.6. For α Cir, we obtained an estimate of $\sim$170 $\mathrm{m\,s^{-1}}$ while the actual cross-correlation measurements gave 168–182 $\mathrm{m\,s^{-1}}$ (depending on the band, numbers 85–88). For HR 3831, we obtained estimates of $\sim$340 and $\sim$290 $\mathrm{m\,s^{-1}}$ for the two frequencies while the actual measurements gave 338–361 and 296–318 $\mathrm{m\,s^{-1}}$ respectively. The good agreement, between the estimates obtained from the bisector analysis and the velocity amplitudes from the cross-correlation measurements (using four different bands), argues that the bisector velocities are accurate.

However, there is a similarity between the α Cir and HR 3831 bisector results (see Fig. 15) that is possibly inconsistent with depth effects being the cause of the bisector variations. This is because the pulsations of these two stars have significantly different periods (7 and 12 min) and, therefore, have different vertical wavelengths, assuming that the sound speed is approximately the same between their atmospheres. If depth effects are causing the bulk of the observed bisector variations, the Hα line is formed over a larger vertical distance, and/or the sound speed is lower, in the atmosphere of HR 3831.

Again, surface effects could explain the bisector variation in α Cir and HR 3831 if they were pulsating in modes with $\ell \geq 3$ (see Hatzes 1996). Therefore, we are left with two relatively

straightforward explanations for the amplitude and phase variations: (i) the stars pulsate in dipole modes and the variations are caused by depth effects; or (ii) they pulsate in $\ell = 3$ modes and the variations are caused by surface effects. A more complicated explanation could involve a combination of standing waves, running waves, surface effects, distorted modes and blending.

6.2 Rotational modulation in HR 3831

There are many examples of rotational modulation shown in this paper. The large variation in the shape of the modulation between different observables was an unexpected result, for which we see three possible explanations.

(1) The oblique pulsator model is wrong and the observed frequency triplet is caused by three different modes.

(2) The oblique pulsator model is correct and the variations are caused by systematic errors in the measurements.

(3) The oblique pulsator model is correct but needs to be modified to include effects arising from spots or some other mechanism.

In the first case, the relative amplitude between different modes would be expected to vary for different observables. This is the natural explanation for the differences between ν_{-1} and ν_{+1} of the metal-line velocity amplitudes and phases (Figs 7 and 8) and of the Hα -width amplitudes and phases (Fig. 16). However, it would require some rotational phase-locking process to account for the frequency separations being equal to the rotation frequency.

In the second case, no simple systematic error could explain the variation in the shape of the rotational modulation. Any such error would need to be varying with the rotation. For instance, a variation in blending could possibly account for the rotational modulation of the metal-line amplitudes and phases, but it could not account for the Hα-width variations.

For the third case, we consider the Hα line because it is the least affected by blending. First, note that the intensity modulation, using a filter with a FWHM of about 6 Å, is fitted well by the rotational modulation derived from the photometric triplet. This means that the *total intensity* variations below a height of about 0.62 are in agreement with the oblique pulsator model. The bisector velocities are also in agreement, so it is only the width variations below 0.62 that are not in agreement with the model. Perhaps this could be explained by hot spots in the upper atmosphere that cause significant amplitude and phase differences between pulsational temperature changes in and around the spots. As the star rotates, the effect on the Hα profile would vary, leading to a hybrid model combining spots with an oblique pulsator.

6.3 Future work

It is clear that the high-resolution study ($R \gtrsim 40\,000$) of different metal lines will be necessary to improve the understanding of the pulsation and the structure of the atmosphere in roAp stars, because of the problems associated with blending at lower resolution ($R \sim 5000$). It will then be possible to compare the velocity amplitudes and phases between different atoms and ionization states. Theoretical work needs to be done to calculate formation depths for individual lines, including the effects of diffusion and the magnetic field. The aim is to build up a coherent picture of the pulsation in the atmosphere.

Of the results on α Cir and HR 3831, the Hα profile measurements are least affected by blending and cannot easily be improved using high-resolution spectroscopy. The profile measurements require a good continuum fit across the Hα line, which is about 100 Å wide in these A stars. For this reason, a spectrum which is stable across at least 400 Å is preferable. This is harder to obtain with high-resolution spectroscopy because of the blaze pattern and the size of CCD detectors. Although improvement could be made on the results using intermediate-resolution spectroscopy ($R \sim 15\,000$), modelling the formation of the Hα line is more important. Determining depth and surface effects on the Hα profile will complement high-resolution spectroscopic and theoretical studies of metal lines.

Photometric oscillation spectra could be considerably improved from observations of roAp stars using small space telescopes. Two such missions plan to include roAp stars as part of a project to measure oscillations in nearby stars (*MONS*[3], see Baldry 1998; and *MOST*[4]). If successful, the project will result in the detection of new modes and improved asteroseismology of the brightest roAp stars.

The spectroscopic study of the pulsations in roAp stars has produced more questions than answers, because of the complexity of the observed spectral changes. For the same reason, the 'amount of information' obtainable is very large (e.g., variations in amplitudes and phases) compared to other pulsating stars. Therefore, roAp stars are prime stellar objects for testing diffusion, magnetic field and pulsation theories.

ACKNOWLEDGMENTS

We would like to thank: Don Kurtz, Jaymie Matthews and Lawrence Cram for helpful discussions; the referee for helpful comments; the MSO staff for observing support; the SAAO staff for photometric data, and the Australian Research Council for financial support.

REFERENCES

Baldry I. K., 1998, in Kjeldsen H., Bedding T. R., eds, Proc. First MONS Workshop, Science with a Small Space Telescope. Aarhus Univ., Denmark, p. 135

Baldry I. K., Bedding T. R., Viskum M., Kjeldsen H., Frandsen S., 1998a, MNRAS, 295, 33 (B98)

Baldry I. K., Kurtz D. W., Bedding T. R., 1998b, MNRAS, 300, L39 (BKB)

Baldry I. K., Viskum M., Bedding T. R., Kjeldsen H., Frandsen S., 1999, MNRAS, 302, 381 (B99)

Dziembowski W. A., Goode P. R., 1985, ApJ, 296, L27

Dziembowski W. A., Goode P. R., 1986, in Gough D. O., eds, Seismology of the Sun and the Distant Stars. Reidel, Dordrecht, p. 441

ESA, 1997, The Hipparcos and Tycho Catalogues, ESA SP-1200. European Space Agency Publ. Division, c/o ESTEC, Noordwijk

Gautschy A., Saio H., Harzenmoser H., 1998, MNRAS, 301, 31

Hatzes A. P., 1996, PASP, 108, 839

Kanaan A., Hatzes A. P., 1998, ApJ, 503, 848

Kurtz D. W., 1982, MNRAS, 200, 807

Kurtz D. W., 1990, ARA&A, 28, 607

Kurtz D. W., Shibahashi H., Goode P. R., 1990, MNRAS, 247, 558

Kurtz D. W., Kanaan A., Martinez P., Tripe P., 1992, MNRAS, 255, 289

[3] Measuring Oscillations in Nearby Stars (`http://www.obs.aau.dk/MONS/`)

[4] Microvariability & Oscillations of STars (`http://www.astro.ubc.ca/MOST/`)

Kurtz D. W., Kanaan A., Martinez P., 1993, MNRAS, 260, 343
Kurtz D. W., Martinez P., van Wyk F., Marang F., Roberts G., 1994a, MNRAS, 268, 641
Kurtz D. W., Sullivan D. J., Martinez P., Tripe P., 1994b, MNRAS, 270, 674
Kurtz D. W., van Wyk F., Roberts G., Marang F., Handler G., Medupe R., Kilkenny D., 1997, MNRAS, 287, 69
Ledoux P., 1951, ApJ, 114, 373
Martinez P., Kurtz D. W., 1995, in Stobie R. S., Whitelock P. A., eds, ASP Conf. Ser., Vol. 83, Astrophysical Applications of Stellar Pulsation. Astron. Soc. Pac., San Francisco, p. 58
Martinez P. et al., 1996, MNRAS, 282, 243
Mathys G., 1985, A&A, 151, 315
Matthews J. M., 1991, PASP, 103, 5
Matthews J. M., 1997, in Provost J., Schmider F. X., eds, Proc. IAU Symp. 181, Sounding Solar and Stellar Interiors. Kluwer, Dordrecht, p. 387
Matthews J. M., Wehlau W. H., Walker G. A. H., Yang S., 1988, ApJ, 324, 1099
Schmidt-Kaler T., 1982, in Schaifers K., Voigt H. H., eds, Landolt-Börnstein, Group VI, Vol. 2b. Springer-Verlag, Berlin, p. 451
Shibahashi H., 1991, in Gough D., Toomre J., eds, Lecture Notes in Physics 388, Challenges to Theories of the Structure of Moderate-Mass Stars. Springer-Verlag, Berlin, p. 393
Shibahashi H., Takata M., 1993, PASJ, 45, 617
Takata M., Shibahashi H., 1994, PASJ, 46, 301
Takata M., Shibahashi H., 1995, PASJ, 47, 219

This paper has been typeset from a TEX/LATEX file prepared by the author.